Accepted for publication in Journal of Adhesion Science and Technology, June 2017

FRACTURE INITIATION IN BI-MATERIAL JOINTS SUBJECT TO COMBINED TENSION AND SHEAR LOADING

A. R. AKISANYA

School of Engineering, University of Aberdeen,
Aberdeen AB24 3UE, U.K.

ABSTRACT

Linear elastic solution of the stress field near an interface corner of bi-material joints is of the form $Hr^{\lambda-1}$, where r is the radial distance from the corner, H is the stress intensity factor and $\lambda-1$ is the order of the singularity. Finite element analysis is used to determine the magnitude of H for a butt joint subject to remote shear; the obtained solution complements existing solution for remote tension and uniform change in temperature. The theoretical solution of the singular shear stress is shown to be in good agreement with the corresponding finite element solution. The effect of combined remote tension, remote shear and uniform change in temperature on the failure loads and failure mechanisms is experimentally determined for brass/araldite/brass butt joint. It is shown that the failure envelope in tensile stress – shear stress space is elliptical and the failure loads decrease with increasing cure temperature due to thermal residual stress associated with the curing process. The application of the results to the assessment of onset of failure in composite patch repair is discussed.

Keywords: Bonded patch repair joints; Corner singularity; Stress intensity factor; Failure initiation; Mixed-mode loading; Thermal stress.

1. INTRODUCTION

The integrity and reliability assessment of bonded joints has received considerable attention for decades due to increasing use of layered solids in wide range of engineering design and patch repair applications. Patch repair is an efficient and cost effective way of extending the service life of damaged engineering structures as it allows a localised in-situ repair of the damaged structure instead of a complete replacement. Patch repair of damaged composite structures involves the removal of sufficient material from the damaged area and replacing the removed material by adhesive bonding of new undamaged repair material to the structure that is being repaired, see for example [1, 2]. Pipes with external corrosion can also be repaired by adhesive bonding of composite overwrap on the external surface of the pipe [3]. Although adhesive bonding of patch repair material provides an efficient load transfer and less stress concentration, the compatibility of the coefficient of thermal expansion between the repair material and the structure being repaired is an essential consideration for the integrity of the patch. The reliability of many bonded patch repair joints depends on the quality of the processing (i.e. the bonding process) and on the stresses developed when the joints are subject to external loads. Consequently there has been a lot of research on the prediction of stress distribution in bonded joints and layered solids, and on the use of the stresses in predicting the onset of failure and in design optimisation.

Earlier studies on the stress distribution in bonded joints are based on classical beam theory [4 - 6] and do not predict the presence of stress singularity which in most cases is the source of failure in bonded joints and fibre-reinforced composites. It is now well known that a stress singularity exists at the interface corners of an elastic, brittle adhesive sandwiched between two elastic adherends. Although the stress singularity vanishes when there is significant non-linear deformation, a strain singularity still exists. A detailed

characterisation of the singularity is essential for accurate prediction of failure initiation in bonded joints and in assessing the life extension of patch repairs.

A typical bonded joint is of the sandwich type where a thin layer of adhesive, weld material or solder is sandwiched between two adherends. Some examples of commonly used bonded joint geometries are shown in Figure 1. In particular, examples of bonded scarf patch repair joints and composite wrap joint are shown in Figures 1e and 1f respectively. For composite wrap joint (Fig. 1f), the new undamaged material is externally bonded via epoxy resin to and wrapped over the structure being repaired. For these joint geometries stress singularities exist at the intersection of the interface with a free surface or at the intersection of two or more interfaces. Following Williams [7] pioneering work on stress singularity near the tip of a crack in a monolithic material, the stress distribution near the interface corner of bi-material joints made from linear elastic materials has been shown to scale as $Hr^{\lambda-1}$, see for example [8-13]. Here r is the radial distance from the interface corner, $\lambda-1$ is the order of the stress singularity which depends on the local geometry at the interface corner and on the materials combination, and H is the interface corner stress intensity factor (sometimes referred to as the generalised stress intensity factor). This asymptotic solution is valid when the radial distance r is small in comparison to other characteristic lengths of the geometry. Solutions for λ exist in the literature for a wide range of interface corner geometries and material combinations; see for example [8-14]; and λ values in the $0 < \lambda < 1$ correspond to singular stress field. For composite patch repairs which involve the bonding of anisotropic materials, λ may be complex [15].

The intensity factor H is related to the applied load, joint geometry and materials elastic properties. Solutions for H determined from full finite element analysis of specific joint

geometry and loading exist in the literature for different materials combinations and bonded joint geometries. For example, a butt joint subjected to remote tension and uniform change in temperature [16, 17] and a lap joint subject to shear load [18].

The use of both H and λ to adequately quantify the asymptotic stresses near the interface corner of bi-material joints is now well established. The focus of many researchers has shifted more recently to the optimal selection of materials for example through the use of functionally graded adhesives [19] and optimal selection of joint geometry [20] to minimise the stress singularity, and also to accurate prediction of onset of fracture in each of these cases [13].

A number of methods have been suggested for predicting the initiation of fracture in bi-materials joints without initial gross defects including patch repairs. These include a shear-lag based approach, where failure is assumed to occur at a critical shear strain in the adhesive [5, 19]; the maximum principal stress criterion [6]; the average normal stress criterion, where failure is assumed to occur when the average stress equals a material dependent critical stress [21, 22]; the strain energy density criterion [23], coupled strength and energy methods [24] and the stress intensity factor approach, e.g. [11, 12, 16].

In the stress intensity factor approach, initiation of fracture is assumed to occur at the interface corner of bonded joints when the intensity factor, H, of the singular elastic stress field at the corner attains a critical value, H_c, provided the dominance zone of the singular stress field is greater than the size of any non-linear deformation or fracture process zone at the corner. This approach, which is similar to the conventional small scale yielding linear elastic fracture mechanics concepts, has been shown to accurately predict the onset of

fracture in a range of bonded joints, for example bonded joints subjected to remote tension and a combined remote tension and temperature change [11, 12, 16]. However, many bonded joint structures and components, including patch repaired structures, are in practice subject to mixed-mode loading, and the suitability of the criterion for predicting fracture initiation in bonded joints with no pre-existing cracks/defects and subject to combined remote tension and shear is not yet clear. Damaged structures that have been repaired by external adhesive bonding of composite wrap (see Fig. 1f) may in service be subject to a combination of remote tension, shear load and uniform change in temperature. In this paper, we examine the initiation of failure from the interface corners of adhesively bonded butt joints with no pre-existing cracks and subjected to combined remote tension and in-plane shear. The failure loads are experimentally measured and the corresponding stress intensity factor is determined.

2. STATEMENT OF THE PROBLEM

Consider a damaged engineering structure made from an isotropic material which is to be patch repaired by adhesive bonding of composite overwrap (see Fig. 1f). For a composite wrap made of woven fibre fabric reinforced polymer or for randomly distributed short fibre reinforced polymer, the composite wrap can be assumed to be isotropic or quasi-isotropic. In order to assess the initiation of failure from the interface corner of such composite patch repair, we consider in this paper a butt joint consisting of two isotropic, linear elastic materials as shown in Figure 2. A thin layer of adhesive material (material 2) with thickness h is sandwiched between two adherends (material 1). Here the adhesive is the material used to bond the patch repair material to the structure that is being repaired. The materials have a Young's modulus E, Poisson's ratio ν and coefficient of thermal expansion α. The elastic and thermal properties associated with the adherend material are

identified with subscript 1 while those associated with the adhesive material are identified with subscript 2. The width of the joint is w and the total length is $2L$. The thickness h of the adhesive is much smaller than any other dimensions of the geometry, i.e. $h << w$, $h << L$, and $L >> w$. The joint is subject to remote stress σ^{∞}, shear stress τ^{∞}, and a uniform change in temperature ΔT, as shown in Fig. 2.

The asymptotic singular stress field at one of the four interface corners of the joint is given by [10, 17, 25]

$$\sigma_{ij} = Hr^{\lambda-1} f_{ij} + \Sigma_{ij} \tag{2}$$

where $(i, j) \equiv (r, \theta)$ are plane polar co-ordinates centred at the interface corner of interest (see Fig. 2); λ–1 is the order of the stress singularity; f_{ij} are non-dimensional functions of θ; Σ_{ij} are components of a uniform stress field associated with temperature change, and H is the interface corner stress intensity factor. The solution of f_{ij} and Σ_{ij} for butt and scarf joints are given in [25]. The intensity factor H is defined such that $\sigma_{\theta\theta}(r, \theta = 0) = Hr^{\lambda-1}$ and it is related to the joint geometry and the remotely applied loads (assuming linear superposition) by

$$\begin{aligned} H &= H_{\sigma} + H_{\tau} + H_{\Delta T} \\ &= h^{1-\lambda}\left(\sigma^{\infty} Q_{\sigma} + \tau^{\infty} Q_{\tau} + \sigma_o Q_{\Delta T}\right) \end{aligned} \tag{3}$$

where σ_o is the stress associated with the temperature change which, for plane strain deformation, is related to the elastic and thermal properties according to [22]

$$\sigma_o = 2.\Delta T.\left[\alpha_2(1+\nu_2) - \alpha_1(1+\nu_1)\right]\left[\frac{1-\nu_1^2}{E_1} + \frac{1-\nu_2^2}{E_2}\right]^{-1} \tag{4}$$

In eqns. (3) and (4) above, α is the coefficient of linear thermal expansion, and Q is a non-dimensional constant function of the materials elastic properties. Qian and Akisanya [25]

have determined Q_σ and $Q_{\Delta T}$ for sandwiched butt joint while the values of Q_τ are given by Reedy [26], Wang and Rose [27] and Van Tooren [18] for lap joints consisting of a thin layer of adhesive sandwiched between rigid adherends. In the current paper, the solution of Q_τ is determined for a range of material combination using the finite element method. The linear superposition of the stress intensity factor solution given in (3) which is a consequent of the linear elastic analysis has been shown to agree reasonably well with experimental results of a butt and scarf adhesive joints subject to combined remote tension and uniform change in temperature [16, 25]. Failure occurs when the stress intensity factor *H* attains a critical value H_c; H_c which is determined by experiment is a function of the material combination, joint geometry and joint processing parameters, e.g. surface preparation.

3. EXPERIMENTS

3.1 *Materials and specimen preparation*

Butt joint specimens were made from brass (composition 60 wt% copper, 40 wt% zinc) and a two-pack araldite as the epoxy adhesive. Uniaxial tensile test using dog-bone specimens was carried out on the brass at a strain rate of 10^{-3} s^{-1} and on the two-part araldite cured at room temperature for 24 hours at a uniaxial strain rate of 6×10^{-4} s^{-1}. The Young's modulus, yield stress and tensile strength were found to be 88 GPa, 200 MPa and 386 MPa respectively for the brass, and 2.1 GPa, 10 MPa and 14 MPa respectively for the araldite. The Poisson's ratio was taken to be $\nu = 0.33$ for the brass and $\nu = 0.35$ for the araldite while the coefficient of linear thermal expansion was 5.8×10^{-5}/K for the araldite [16] and 19×10^{-5}/K for the brass [28].

Each of the brass adherends for the butt joint was 50 mm long, 5 mm thick and 30 mm wide, with a 12.5 mm diameter hole at the distal end for attachment to the loading fixtures.

The bonding surface of the brass was polished using silicon carbide emery paper (P400 grit) and degreased with acetone. The two-pack araldite was mixed thoroughly in ratio 1:1 and applied to the bonding surfaces. The two halves of the specimens were carefully clamped together in order to eliminate air bubbles and a nominal layer thickness of $h \approx 1$ mm was maintained by applying a slight end pressure. In order to examine the effect of thermal residual stress, the adhesive joints were cured in air for 24 hours at different temperatures: room temperature ($\approx 20\ ^{o}$C), $40\ ^{o}$C, $80\ ^{o}$C and $120\ ^{o}$C. Subsequently, the layer thickness was measured using travelling microscope at five different points along the width of the joint; only specimens where all the five measurements of the layer thickness were within the range of 0.85 mm and 1.3 mm were tested.

3.2 Test procedure

The bonded joint specimens were loaded using the Arcan load fixture arrangement shown in Fig. 3 [29, 30]. Different mode-mixity was applied to the joint by varying the angle Φ between the direction of loading and the normal to the interface of the butt joint; Φ was varied between 0^{o} and 90^{o}. Three nominally identical butt joint specimens were tested at each load angle Φ; all the tests were carried out at room temperature. Note that $\Phi = 0^{o}$ corresponds to remote tension loading with no remote shear, while $\Phi = 90^{o}$ corresponds to remote shear loading with no remote tension. The test was carried out at room temperature using standard screw-driven test machine in displacement control and at a cross-head speed of 1 mm/min. The applied load and the displacement were continuously monitored using a computerised data logger.

3.2 Load versus displacement response and failure mechanisms

Typical load versus displacement response for the joint is shown in Figure 4 for the cold cured specimens and in Figure 5 for specimens cured at 40 ^{o}C. The response for small loading angle ($\Phi < 30^{o}$) is linear up to the initiation of failure, while for greater loading angle the response is initially linear and then nonlinear as the failure load is approached. The loading angle for the transition from linear response to non-linear response decreases with increasing cure temperature of the adhesive, see Figures 4 and 5. The load at failure increases with increasing magnitude of the loading angle Φ. There is relatively small scatter in the response and in the failure load for each set of three nominally identical specimens tested at each loading angle; this is an indication of the reproducibility of the test results.

The failure load for the hot cured specimens is lower than for the corresponding cold cured specimens. The thermal residual stress associated with the curing process reduces the external mechanical load required for failure initiation in the joints [14]. The failure tensile stress – shear stress space is shown in Figure 6. The average failure stress when the joint was loaded under pure remote shear is almost three to four times greater than the average failure stress when loaded in uniaxial tension for all the curing conditions considered. Irrespective of the cure temperature of the adhesive, the maximum tensile stress at failure occurred at a loading angle Φ between 30^{o} and 45^{o}. This suggests therefore that the scarf patch repair subject to remote tension the scarf angle for the patch repair should be between 30^{o} and 45^{o} to maximise the load carrying capacity of the repaired structure.

The failure of the joints initiated from interface corners A or D and crack growth occurred either along the interface or within the adhesive (i.e. cohesive failure) depending on the loading angle and the cure temperature as shown in Figure 7. Adhesive cohesive failure occurred when the remote load is predominantly tensile while crack growth occurred along the interface when the remote load is predominantly shear stress (Fig. 7). The observed failure mechanism is consistent with previous work on crack path selection in adhesive joints; increasing magnitude of remote shear results in interfacial crack growth [31].

4. FINITE ELEMENT ANALYSIS OF THE JOINT

In order to determine the critical stress intensity factor at failure, the intensity factor associated with each mode of loading has to be evaluated. The stress intensity factor H for a given magnitude of remote tension σ^{∞}, shear stress τ^{∞} and temperature change ΔT is given in eqn. (3). The stress intensity factors associated with remote tension σ^{∞} and temperature change ΔT have been determined for a wide range of material combination in a separate study [16, 25]. For the elastic properties of the brass and araldite given earlier and the butt joint geometry under consideration: $\lambda = 0.698$, $Q_{\sigma} = 0.445$ and $Q_{\Delta T} = -0.395$ [16, 25]. From (3) and (4), for a material combination where $\alpha_2(1+\nu_2) > \alpha_1(1+\nu_1)$, a negative $Q_{\Delta T}$ when there is a uniform increase in temperature implies a negative intensity factor H and a compressive thermal residual stress at the interface corner. This consequently enhances the additional externally applied load required for failure.

The non-dimensional constant Q_{τ} associated with the remotely applied shear stress τ^{∞} is determined in the current study for the butt joint shown in Figure 2a by performing an elastic finite element analysis of the joint using the general purpose finite element code

ABAQUS. The layer thickness was taken as $h = 1$ unit, and the other dimensions were: $w = 10h$ and $L = 21h$. Eight-node quadrilateral plane strain elements with a refined mesh at the interface corners were used. The materials were considered to be linear elastic with identical Poisson's ratio $\nu = 0.33$, and the relative modulus of the adherend to that of the adhesive, E_1/E_2, was varied between 1 and 200.

The magnitude of the stress intensity factor H_τ and hence of the non-dimensional constant Q_τ were determined from the finite element solution of the stresses and displacements near interface corner A using Betti reciprocal theorem based contour integral method [9, 25]. This method has been shown to be more accurate than the method of matching the finite element stress solution with the asymptotic solution, as the contour integral approach allows the determination of the intensity factor from stress and displacement solutions away from the singular point [25].

The values of Q_τ are shown in Figure 8 as a function of E_1/E_2. We note that the value of Q_τ decreases with increasing value of $E_1/E_2 > 1.5$. For the brass/araldite/brass butt joint under consideration where $E_1/E_2 = 42$, we obtained $Q_\tau = -0.807$ for the non-dimensional constant defined in eqn. (3). It is important to note that the stress intensity factor H_τ associated with remote shear traction τ^∞ is negative at the interface corners A and D, and positive at interface corners B and C, for the butt joint geometry and loading shown in Figure 2. Whether Q_τ is negative or positive at a given interface corner, say A (see Fig 2) depends on the orientation of the coordinate axes; the sign of Q_τ provides an indication of the direction of the singular shear stress at the interface corner. If the orientation of the coordinate axes at corner A as shown in Figure 2 was reversed, the sign of Q_τ would be

reversed too. The solution for Q_τ presented in Figure 8, together with the corresponding solution for Q_σ and $Q_{\Delta T}$ presented in [25] will allow the interface corner stress intensity factor H to be determined for a butt joint subjected to a combination of remote tension, remote shear and a uniform change in temperature.

Reedy [26] and Wang and Rose [27] determined the magnitude of Q_τ for a lap joint consisting of an elastic adhesive layer sandwiched between rigid adherends and subject to shear load, by matching the finite element displacement [26] or stress [27] solution near an interface corner to the corresponding asymptotic solution. Wang and Rose [27] calibration of the stress intensity factor H is similar to that given in (3). However, the solution of H provided by Reedy [26] must be multiplied by $(0.5)^{1-\lambda}$ to ensure the same definition for H as that given in eqn. (3). Using the Poisson's ratio $\nu = 0.35$ for the araldite considered in the current investigation, both Reedy [26] and Wang and Rose [27] simulations gave $Q_\tau = -0.969$ at the interface corner of a lap joint consisting of elastic adhesive sandwiched between rigid adherends and subject to remote shear load. In the current study of a butt joint, an adherend with a Young's modulus $E_1 = 200E_2$ where E_2 is the Young's modulus of the adhesive is considered to be a rigid adherend. For a butt joint with $E_1 = 200E_2$, we obtain $Q_\tau = -0.945$. It is surprising to note that for adherends which are relatively rigid in comparison to the adhesive, the magnitude of the intensity factor at the interface corner for a butt joint subject to remote shear is only about 3% less than that for a lap joint subject to shear load.

With the non-dimensional constant Q_τ due to remote shear determined for the butt joint and materials combination, the intensity factor H can be calculated using eqn. (3) and the asymptotic stresses determined from eqn. (2). Figure 9 shows the comparison of the finite

element and asymptotic solutions of the shear stress $\tau_{r\theta}$ distribution along different angular direction for a butt joint with $E_1 = 200E_2$ and subject to remote shear τ^{∞} without any applied remote tension or temperature change. The asymptotic solution is based on eqns. (2) and (3). There is very good agreement between the finite element and the asymptotic solutions very near the interface corner up to a radial distance $r = 0.03h$ from the interface corner; the two solution starts to diverge as expected as the distance from the interface corner increases. The onset of the deviation of the finite element solution from the asymptotic solution determines the region of validity of the asymptotic solution.

The non-dimensional constant Q_τ associated with remote shear load determined in this paper when combined with the previously determined constants Q_σ and $Q_{\Delta T}$ for remote tension and uniform temperature change in eqn. (3) will enable an assessment of the combination of shear load, tensile load and temperature change required for the initiation of failure at the interface corner of a bonded patch repair joint. We note that the load – displacement response may in practice be slightly non-linear at high loading angle, see Figures 4 and 5, while the application of the stress intensity factor based approach in eqn. (3) is based on linear elastic deformation. However, it has been shown that the critical stress intensity factor is a valid fracture parameter even when there is non-linear deformation at the interface corner provided the plastic zone size is less than the extent of the elastic singular stress field [12]. For a butt joint between two materials that have identical Poisson's ratio, $\nu_1 = \nu_2$, the critical stress intensity factor H_c is a valid fracture parameter when $13\left(H_c / \sigma_Y\right)^{1/(1-\lambda)} < h$ where σ_Y and h are the yield stress and thickness of the adhesive material [12].

5. CONCLUSIONS

The failure envelope of a brass/araldite/brass butt joint subjected to a combination of remote tension, remote shear and uniform change in temperature has been experimentally determined. The failure envelope is found to be a function of the cure temperature of the adhesive; the failure loads decrease with increasing cure temperature due to the presence of thermal residual stress.

The stresses near the interface corner of bonded joints are fully characterised by the interface corner stress intensity factor H and the order of the elastic singularity, $\lambda-1$. Solution of the stress intensity factor at the interface corner of the butt joint due to remote shear has been obtained to complement existing solution for remote tension and uniform change in temperature. The accuracy and validity of the interface corner stress intensity facture due to remote shear is ascertained by the good comparison that was obtained between theoretical and elastic finite element solutions near the interface corner. The solution presented in this paper will enable better prediction of failure of butt joints and patch repaired joints, in particular those involving the use of isotropic or quasi-isotropic composites for patch repairs, and subject to a combined remote tension, remote shear and uniform change in temperature.

ACKNOWLWDGEMENT

The author acknowledges David Reid and Mark Gourlay for assistance with the experiments.

REFERENCES

[1] Breitzman TD, Iarve EV, Cook BM, Schoeppner GA, Lipton RP. Optimization of a composite scarf repair patch under tensile loading. Composites: Part A 2009; 40:1921-1930

[2] Wang CH, Gunnion AJ. Optimum shapes of scarf repairs. Composites: Part A 2009; 40:1409-1418.

[3] Duell JM, Wilson JM, Kessler MR. Analysis of a carbon composite overwrap pipeline repair system. Int. J. Pressure Vessels and Piping 2008; 85:782-788.

[4] Goland M, Reissner E. The stresses in cemented joints. J. Appl. Mech. 1944; 11:A17-A27.

[5] Hart-Smith LJ. Further development in the design and analysis of adhesive bonded structural joints. ASTM STP. 1981; 749:3-31

[6] Adam R, Comyn J, Wake W. Structural adhesives joints in engineering. Springer: Berlin; 1997.

[7] Williams ML. Stress singularities resulting from various boundary conditions in angular corners of plates in extension. J. Appl. Mech. 1952; 19: 526-528.

[8] Bogy DB. Two edge-bonded elastic wedges of different materials and wedge angles under surface tractions. J. Appl. Mech. 1971; 38: 377-386.

[9] Carpenter WC, Byers C. A path independent integral for computing stress intensities for V-notched cracks in bi-materials. Int J. Fract. 1987; 35: 245-268.

[10] Reedy ED. Asymptotic interface corner solutions for butt tensile joints. Int. J. Solids Struct. 1993; 30: 767-777.

[11] Munz D, Yang YY. Stresses near the edge of bonded dissimilar materials described by two stress intensity factors. Int. J. Fract. 1993; 60: 169-177.

[12] Akisanya AR, Meng CS. Initiation of fracture at the interface corner of bi-material joints. J. Mech. Phys. Solids. 2003; 51: 27-46.

[13] Weiβgraeber P, Leguillon D, Becker W. A review of finite fracture mechanics: crack initiation at singular and non-singular stress raisers. Arch. Appl. Mech. 2016; 86: 375-401.

[14] Kelly PA, Hills DA, Nowell D. the design of joints between elastically dissimilar components (with special reference to ceramic/metal joints). J. Strain Analysis. 1992; 27: 15-20.

[15] Wang SS, Choi I. Boundary-layer effects in composite laminates: Part 1 – free-edge stress singularities. J. Appl. Mech. 1982; 49:541-548.

[16] Qian Z, Akisanya AR. An experimental investigation of failure initiation in bonded joints. Acta Mater. 1998; 46: 4895-4904.

[17] Yang YY, Munz D. Stress intensity factor and stress distribution in a joint with an interface corner under thermal and mechanical loading. Comp. Struct. 1995; 57: 467-476.

[18] van Tooren MJL, Gleich DM, Beukers A. Experimental verification of a stress singularity model to predict the effect of bondline thickness on joint strength. J. Adh. Sci. Tech. 2004; 18: 395-412.

[19] Kumar S. Khan MA. A shear-lag model for functionally graded adhesive anchors. Int. J. Adhesion Adhesives. 2016; 68: 317-325.

[20] Wu Z. Design free of singularities for bi-material components. Comp Struct. 2004; 65:339-345.

[21] Novozhilov V. On a necessary and sufficient condition for brittle strength. J. Appl. Math. Mech. 1969; 33: 201-210.

[22] Seweryn A. Brittle fracture criterion for structures with sharp notches. Eng. Fract Mech. 1994; 47: 673-681.

[23] Yosibash Z, Bussiba A. Gilad I. Failure criteria for brittle elastic materials. Int. J. Fract. 2004; 125: 307-333.

[24] Leguillon D. Strength or toughness? A criterion fro crack onset at a notch. Euro J. Mech. A Solids. 2002; 21: 61-72.

[25] Qian ZQ, Akisanya AR. Analysis of free-edge stress and displacement fields in scarf joints subject to uniform change in temperature. Fat. Fract. Eng. Mater. Struct. 1998; 21: 687-703.

[26] Reedy Jr. ED. Intensity of stress singularity at the interface corner of a bonded elastic layer subjected to shear. Eng. Fract. Mech. 1991; 38: 273-281.

[27] Wang CH, Rose LRF. Compact solutions for the corner singularity in bonded lap joints. Int. J. Adhesion Adhesives 2000; 20: 145-154.

[28] Ashby MF. Materials selection in mechanical design. 4th edition. Butterworth Heinemann, 2011.

[29] Arcan L, Arcan M, Daniel I. SEM fractography of pure and mixed mode interlaminar fracture in graphite/epoxy composites. ASTM STP. 1987; 948: 41-47.

[30] Stamoulis G, Carrere N, Cognard TY, Davies P, Badulescu C. Investigating the fracture behaviour of adhesively bonded metallic joints using Arcan fixture. Int. J. Adhesion Adhesives. 2016; 66: 147-159.

[31] Akisanya AR, Fleck NA. Brittle fracture of adhesive joints. Int. J. Fract. 1992; 58: 93-114.

FIGURE CAPTIONS

Figure 1: Some examples of bi-material bonded joints with the shaded region indicating the adhesive. (a) Scarf joint, (b) single lap joint, (c) double lap joint, (d) butt joint with square edge, (e) scarf patch repair joint, and (f) composite overwrap patch repair joint.

Figure 2: (a) A schematic of a butt joint subjected to remote tension and shear loads, and (b) a magnified view of the interface corner A showing the local polar coordinates.

Figure 3: A schematic diagram of the Arcan loading configuration

Figure 4: Effect of loading angle Φ on the load versus displacement response of brass/araldite/brass butt joints cured for 24 hours at room temperature (20 ^{o}C).

Figure 5: Effect of loading angle Φ on the load versus displacement response of brass/araldite/brass butt joints cured for 24 hours at a temperature of 40 ^{o}C.

Figure 6: Failure envelope of the brass/araldite/brass joint for different cure temperature.

Figure 7: Effect of loading angle Φ and cure temperature on the failure mechanism map of the brass/araldite/brass joint.

Figure 8: Effect of relative modulus the adherend E_1 to the modulus of the adhesive E_2 on the non-dimensional constant Q_τ.

Figure 9: Elastic finite element and asymptotic solution for $\tau_{r\theta}$ along various radial directions for a butt joint consisting of an adherend with Young's modulus $E_1 = 200E_2$ where E_2 is the modulus of the adhesive. The shear stress $\tau_{r\theta}$ is normalised by the remote shear stress τ^{∞} while the radial distance r is normalised by the layer thickness h. The solid lines are the finite element solution and the dashed-dashed lines are the asymptotic solution.

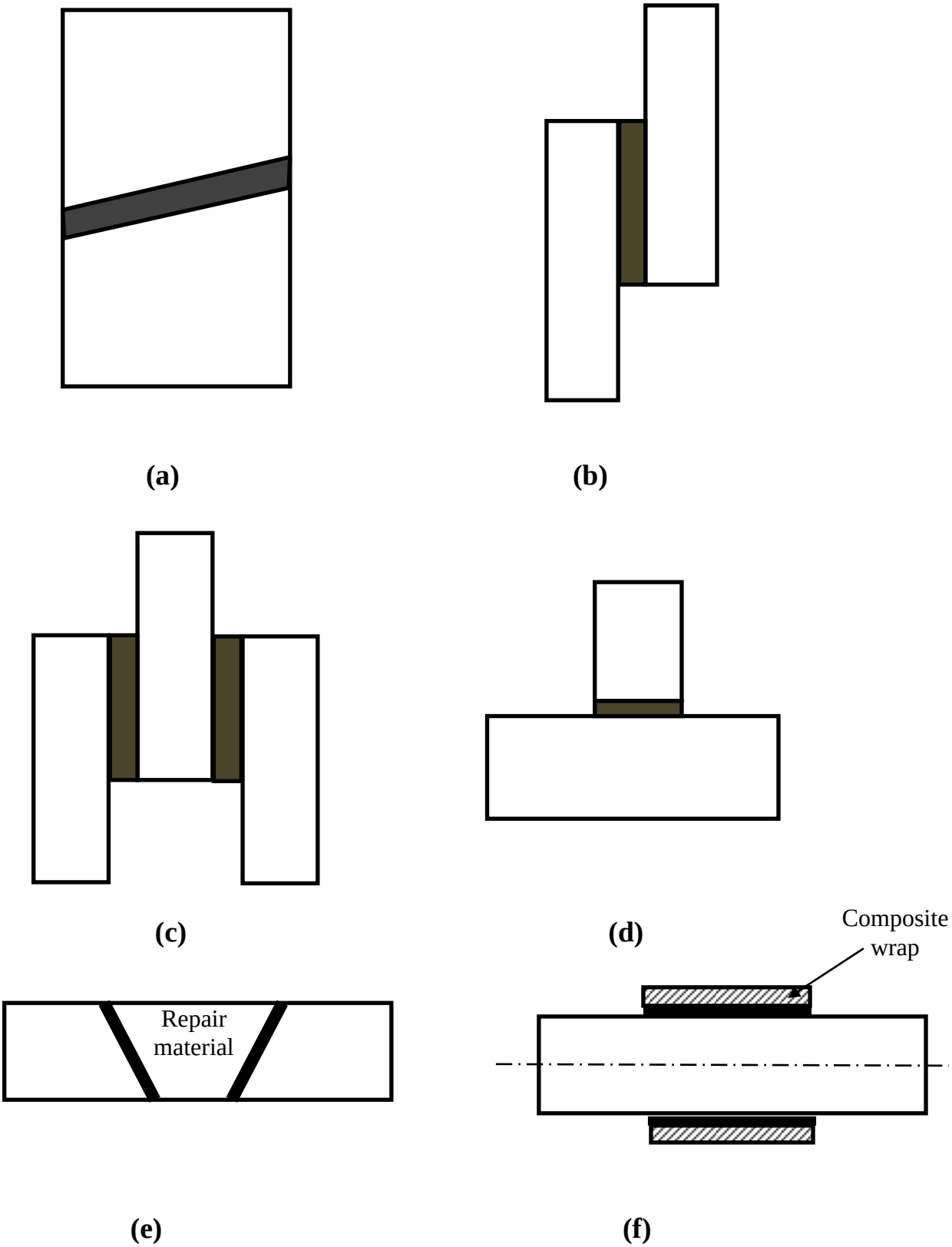

Figure 1: Some examples of bi-material bonded joints with the shaded region indicating the adhesive. (a) Scarf joint, (b) single lap joint, (c) double lap joint, (d) butt joint with square edge, (e) scarf patch repair joint, and (f) composite overwrap patch repair joint.

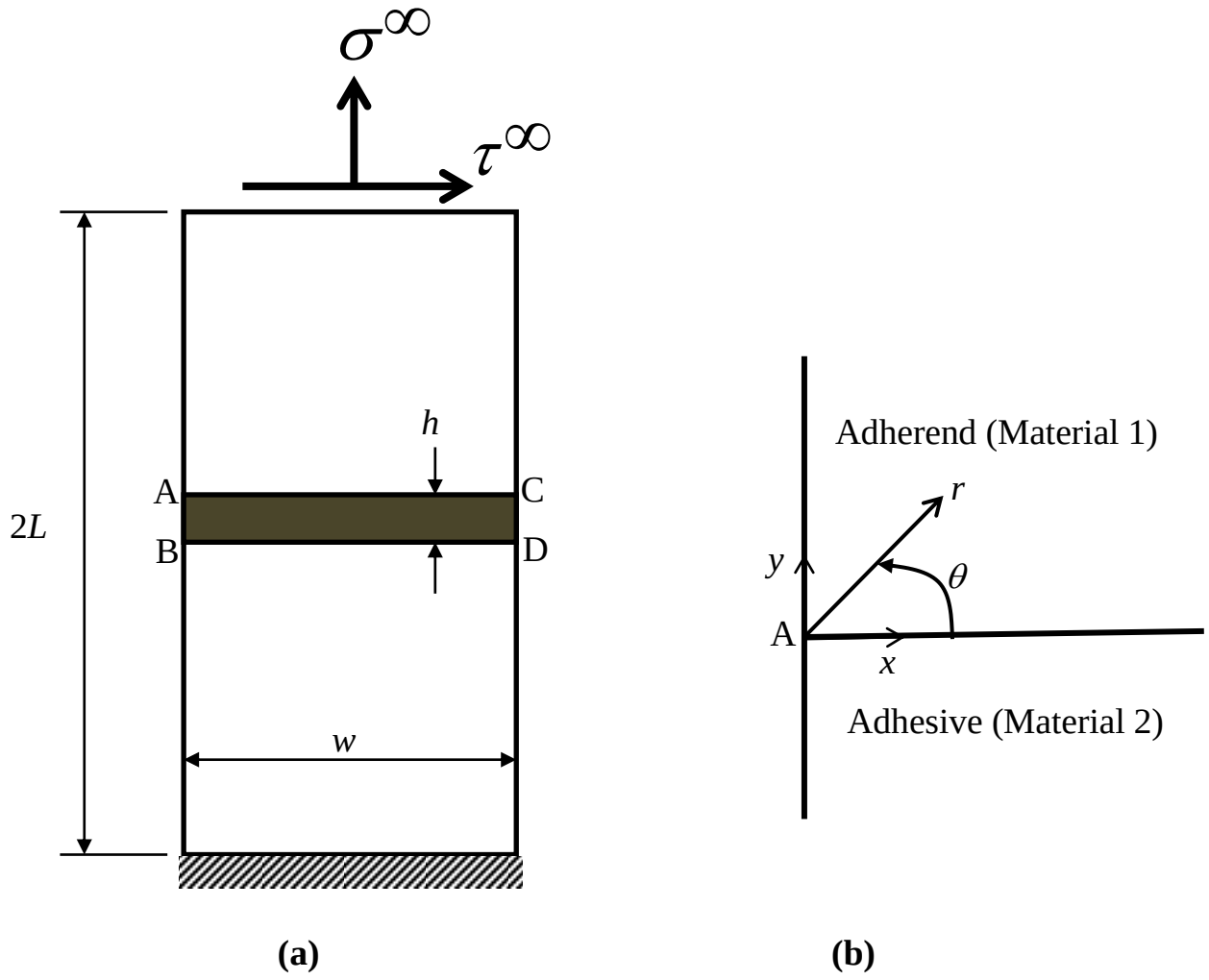

Figure 2: (a) A schematic of a butt joint subjected to remote tension and shear loads, and (b) a magnified view of the interface corner A showing the local polar coordinates.

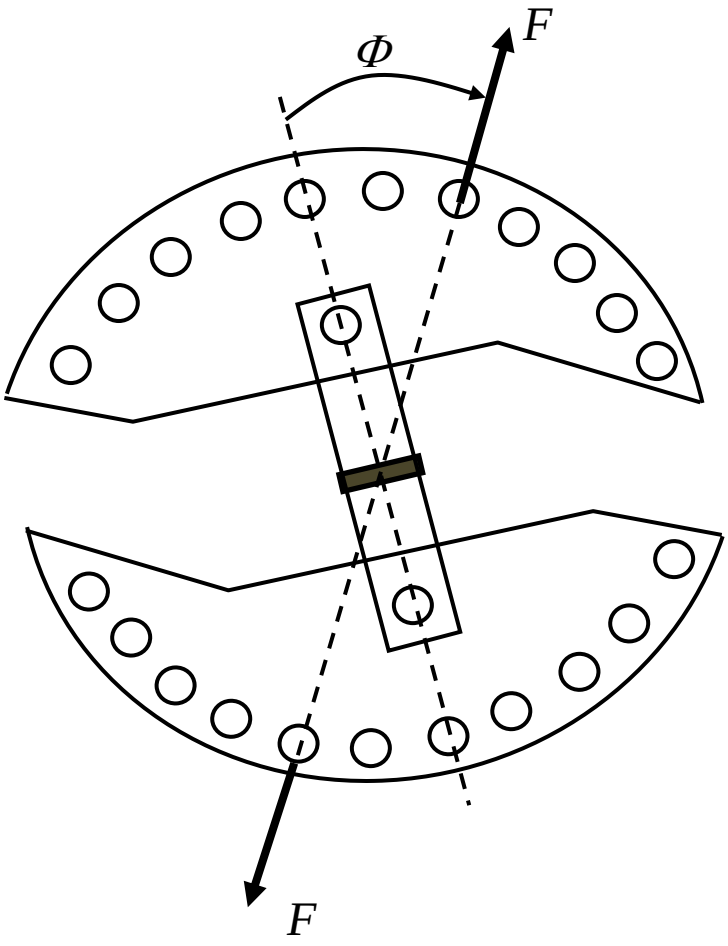

Figure 3: A schematic diagram of the Arcan loading configuration

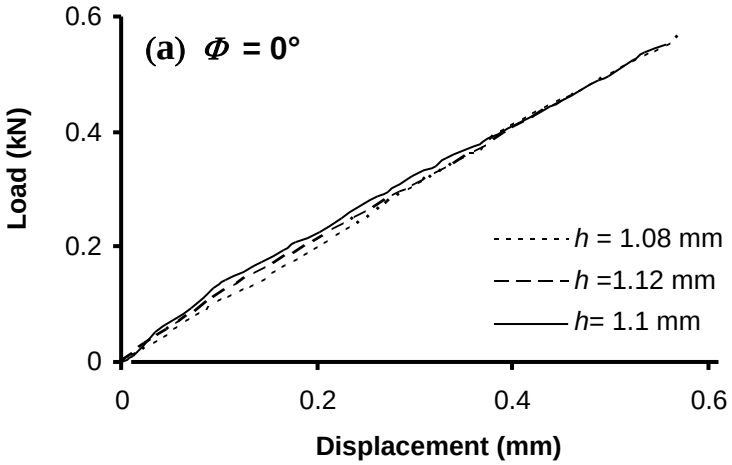

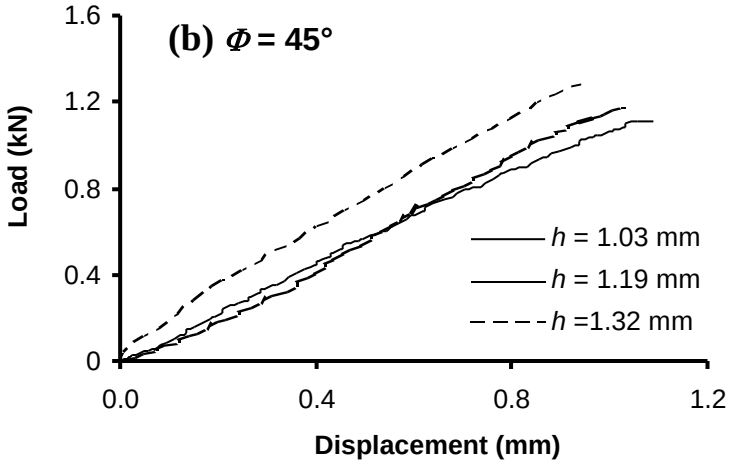

Figure 4a & 4b;
Caption overleaf

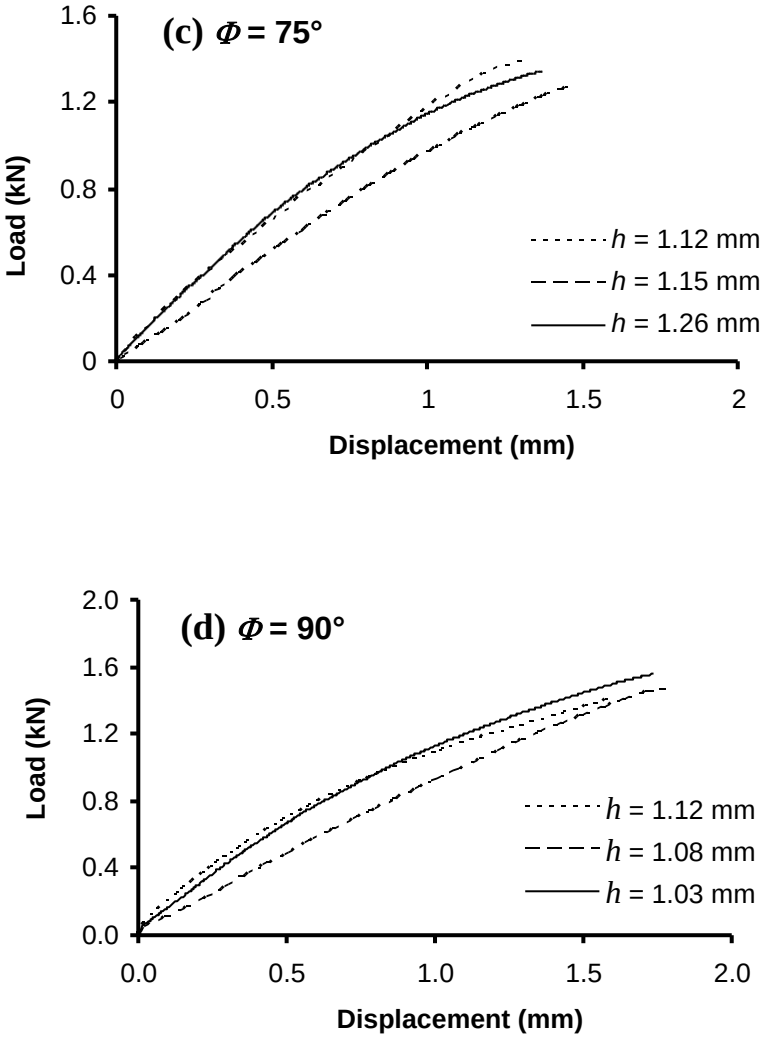

Figure 4: Effect of loading angle Φ on the load versus displacement response of brass/araldite/brass butt joints cured for 24 hours at room temperature (20 ^{o}C).

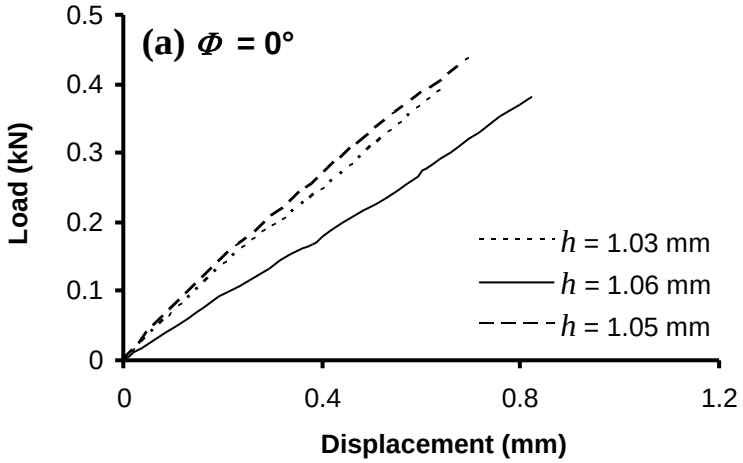

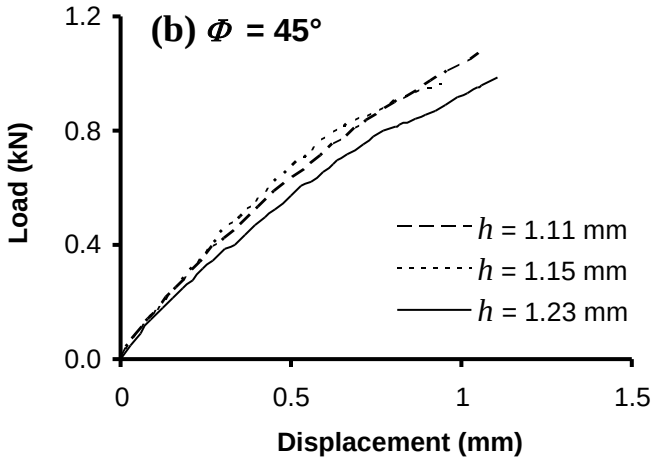

Figure 5a & 5b;
Caption overleaf

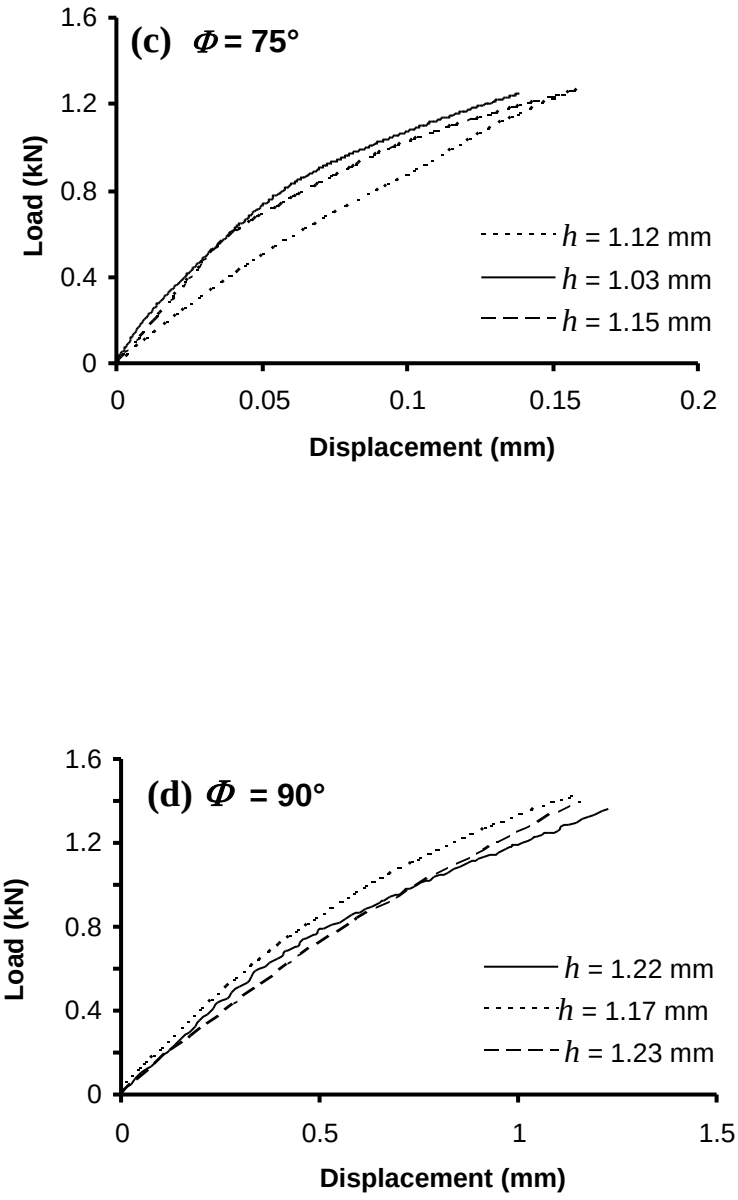

Figure 5: Effect of loading angle Φ on the load versus displacement response of brass/araldite/brass butt joints cured for 24 hours at a temperature of 40 ^{o}C.

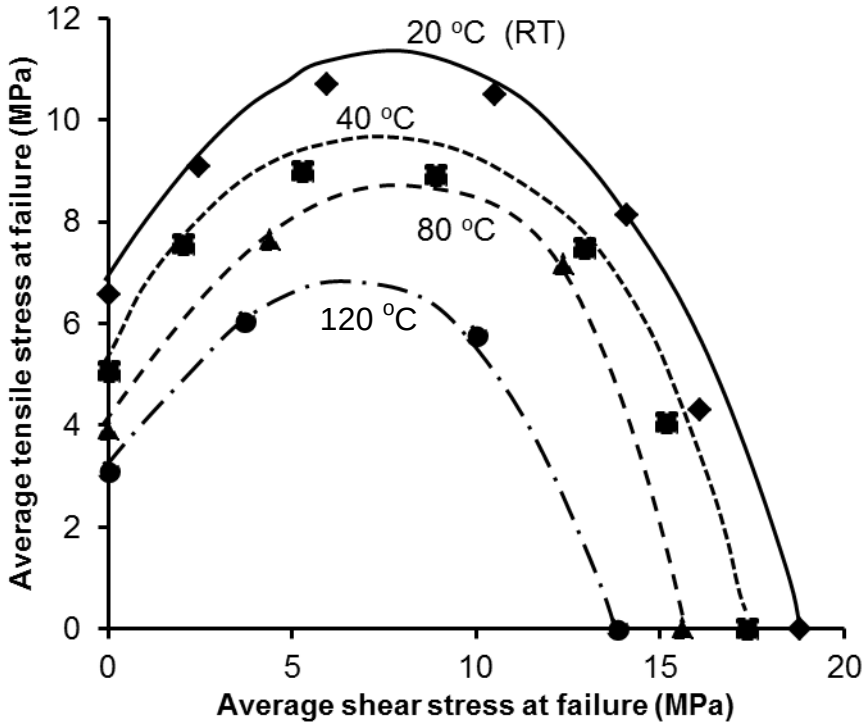

Figure 6: Failure envelope of the brass/araldite/brass joint for different cure temperature.

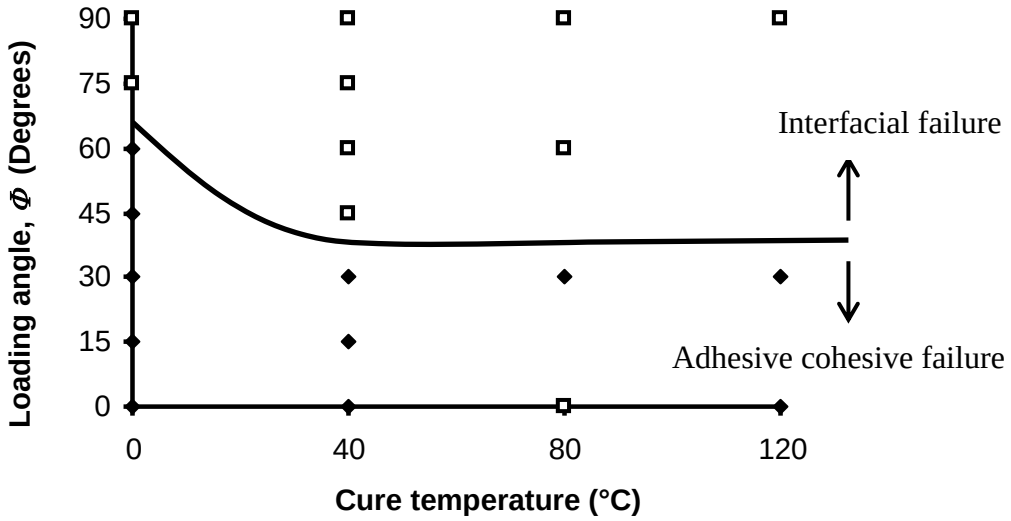

Figure 7: Effect of loading angle Φ and cure temperature on the failure mechanism map of the brass/araldite/brass joint.

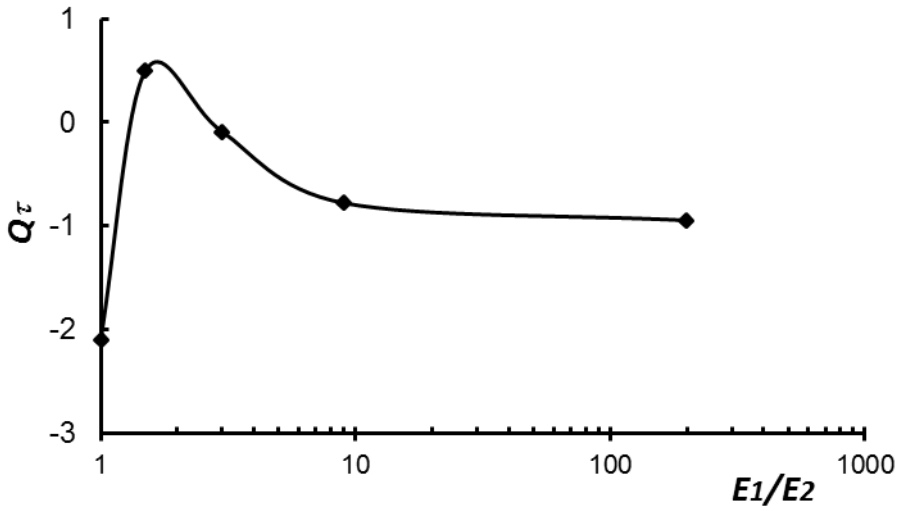

Figure 8: Effect of relative modulus the adherend E_1 to the modulus of the adhesive E_2 on the non-dimensional constant Q_τ.

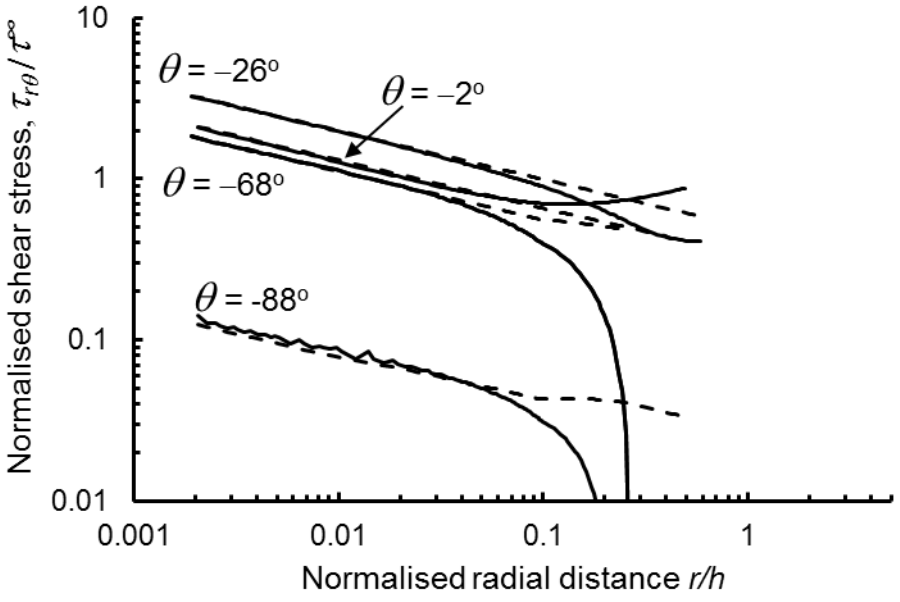

Figure 9: Elastic finite element and asymptotic solution for $\tau_{r\theta}$ along various radial directions for a butt joint consisting of an adherend with Young's modulus $E_1 = 200E_2$ where E_2 is the modulus of the adhesive. The shear stress $\tau_{r\theta}$ is normalised by the remote shear stress τ^{∞} while the radial distance r is normalised by the layer thickness h. The solid lines are the finite element solution and the dashed-dashed lines are the asymptotic solution.